

Quantum Mollow Quadruplet in Nonlinear Cavity QED

Thomas Allcock, Wolfgang Langbein , and Egor A. Muljarov

School of Physics and Astronomy, Cardiff University, The Parade, Cardiff CF24 3AA, United Kingdom

 (Received 18 August 2021; accepted 7 February 2022; published 24 March 2022)

We develop an exact analytical approach to the optical response of a two-level system coupled to a microcavity for arbitrary excitation strengths. The response is determined in terms of the complex amplitudes of transitions between the rungs of the Jaynes-Cummings ladder, explicitly isolating nonlinearities of different orders. Increasing the pulse area of the excitation field, we demonstrate the formation of a quantum Mollow quadruplet (QMQ), quantizing the semiclassical Mollow triplet into a coherent superposition of a large number of transitions between rungs of the ladder, with inner and outer doublets of the QMQ formed by densely lying inner and outer quantum transitions between the split rungs. Remarkably, a closed-form analytic approximation for the QMQ of any order of nonlinearity is found in the high-field low-damping limit.

DOI: [10.1103/PhysRevLett.128.123602](https://doi.org/10.1103/PhysRevLett.128.123602)

The strong coupling regime of cavity quantum electrodynamics (QED), in which light-matter interaction dominates over any dissipation processes, is of both fundamental and technological interest. It gives rise to a formation of mixed states of light and matter, called polaritons [1], and to observation of characteristic vacuum Rabi splitting [2,3]. The latter, being recently observed also in semiconductor quantum dots (QDs) coupled to an optical cavity mode (CM) [4,5], is often referred to as linear classical effect which can be studied by linear optics. In a widely used two-level model of a QD, localized excitons are treated as fermions coupled to a bosonic CM. This coupling introduces a quantum nonlinearity [6,7], which results in an effective photon-photon interaction [8] that can naturally be observed in nonlinear optical spectroscopy [9,10].

The interaction of a two-level system with a single bosonic CM is described by the Jaynes-Cummings (JC) model [11]. The eigenstates of the system form a JC ladder, with a splitting of the polariton-like doublet within each rung proportional to the square root of the rung number. The increasing higher rung splitting is evidence for quantum nonlinearity and quantum strong coupling. The latter was observed [10,12] for QD excitons and also in other systems, such as superconducting circuits [6]. A culmination of the quantum strong coupling is a quantum Mollow triplet (MT) forming in optical spectra of QDs with increasing optical excitation. The classical MT [13] has been recently demonstrated in the coherent emission of QDs [14–18]. A theoretical study of the QD emission spectrum under incoherent optical excitation demonstrated a quantum MT formed due to a superposition of higher-rung transitions [19–21]. This incoherent quantum MT in a QD-cavity system was shown [21] to be different from the classical MT, but is hard to observe due to the short cavity lifetime in presently available structures, preventing the

excitation of large photon numbers by the QD. The nonlinear optical response of a coherently excited QD-cavity system is the observable in experimental reach suited for studying the quantum MT.

We focus here on the four-wave mixing (FWM) and higher-order optical nonlinearities, which can be measured by heterodyne spectral interferometry [22]. For excitation with average photon numbers much lower than one, only the first two rungs of the JC ladder are relevant in the FWM response, with six optical transitions fully describing the dynamics of the system, as demonstrated by a good agreement with experiment [10,23,24]. At higher excitations, deviations between theoretical predictions and experimental data have been attributed to higher-rung contributions to nonlinear spectra, where also some signatures of a MT have been reported [23]. This experiment has been recently extended [25] to larger photon numbers and simulated using a time-domain master equation.

In this Letter, we present an exact analytical approach to the nonlinear optical response of a two-level system (TLS) coupled to a cavity excited by a sequence of ultrashort pulses introducing an arbitrary number of cavity photons. A coherent optical pulse brings a cavity from its ground state into a Glauber coherent state, and its subsequent dynamics is rigorously represented by a superposition of optical transitions between the states of the JC ladder. At higher excitations, the interference of a large number of these transitions gradually transforms the nonlinear spectrum into a coherent quantum Mollow quadruplet (QMQ). To demonstrate this, we calculate the quantum dynamics with multiple precision arithmetic (see Sec. S.VII of the Supplemental Material [26]). We provide a visualization of QMQ formation in the coherent dynamics involving an increasing number of rungs with increasing excitation. We furthermore present an analytic approximation in the

low-damping limit, providing a closed-form solution for the nonlinear optical response of any order. It proves that the line splitting and the linewidth of the outer (inner) doublet of the QMQ observed in nonlinear spectra are given, respectively, by $4\sqrt{n}g$ (g/\sqrt{n}) and $4g$ (g/n), where n is the average number of excited cavity photons and g is the TLS-cavity coupling strength.

Let us start with the TLS-cavity dynamics described [10,24,35] by the master equation (taking $\hbar = 1$)

$$i\dot{\rho} = \hat{L}\rho + [V(t), \rho], \quad (1)$$

where ρ is the density matrix (DM) and the Lindblad super-operator \hat{L} is given by

$$\begin{aligned} \hat{L}\rho = & [H, \rho] - i\gamma_X(d^\dagger d\rho + \rho d^\dagger d - 2d\rho d^\dagger) \\ & - i\gamma_C(a^\dagger a\rho + \rho a^\dagger a - 2a\rho a^\dagger). \end{aligned} \quad (2)$$

Here, H is the JC Hamiltonian of the TLS (e.g., a QD exciton) coupled to a cavity, and γ_X and γ_C are, respectively, the TLS and CM decay rates (for discussion of the parameters of the JC model see the Supplemental Material [26], Sec. S.II),

$$H = \Omega_X d^\dagger d + \Omega_C a^\dagger a + g(d^\dagger a + a^\dagger d), \quad (3)$$

d^\dagger and d are the creation and annihilation operators of the TLS, while a^\dagger and a are those for the CM, having complex eigenfrequencies $\omega_X = \Omega_X - i\gamma_X$ and $\omega_C = \Omega_C - i\gamma_C$, respectively. The dipole coupling of the CM to the external classical electric field $\mathcal{E}(t)$ is described in the rotating wave approximation (consistent with the JC model) by the operator

$$V(t) = -\boldsymbol{\mu} \cdot \mathcal{E}(t) a^\dagger - \boldsymbol{\mu}^* \cdot \mathcal{E}^*(t) a, \quad (4)$$

in which $\boldsymbol{\mu}$ is the effective dipole moment of the CM. For the TLS-cavity system excited by a sequence of ultrashort pulses, this interaction is well described by a series of δ functions,

$$\boldsymbol{\mu} \cdot \mathcal{E}(t) = \sum_j E_j \delta(t - t_j), \quad (5)$$

where E_j is the complex amplitude, known as pulse area, of the pulse arriving at time t_j . Excitations by longer pulses and even finite wave packets can be approximated with Eq. (5), as shown in Sec. S.I of the Supplemental Material [26].

For excitations in the form of Eq. (5), the evolution of the DM is given by a time-ordered product of operators acting on the DM, each such operator consisting of a pulse operator $\hat{X}(E_j)$ due to pulse j and a subsequent Lindblad dynamics during time τ between pulses (i.e., $\tau \leq t_{j+1} - t_j$):

$$\rho(t_j + \tau) = e^{-i\hat{L}\tau} \hat{X}(E_j) \rho(t_j - 0_+), \quad (6)$$

where 0_+ is a positive infinitesimal. The pulse operator has the explicit form

$$\hat{X}(E)\rho = e^{i(Ea^\dagger + E^*a)} \rho e^{-i(Ea^\dagger + E^*a)}, \quad (7)$$

in which $e^{i(Ea^\dagger + E^*a)} = e^{-|E|^2/2} e^{iEa^\dagger} e^{iE^*a}$ is a displacement operator transforming the cavity ground state into a Glauber coherent state [36] with the eigenvalue iE , as shown in Sec. S.I of the Supplemental Material [26]. Hence the average number of photons in such a coherent state, given by the expectation value of $a^\dagger a$, is $|E|^2$. Due to the presence of multiple pulses, the system is in general not in the ground state at pulse arrival. To solve this problem analytically, we introduce an extended basis of Fock states $|\nu, n\rangle$ with the occupation numbers $\nu = 0, 1$ for the TLS and $n = 0, 1, 2, \dots$ for the CM. Using this basis, the DM can be written as

$$\rho = \sum_{\nu' n n'} \rho_{\nu' n n'}^{\nu \nu'} |\nu, n\rangle \langle \nu', n'|, \quad (8)$$

so that the total optical polarization takes the form

$$P(t) = \text{Tr}\{\rho(t)a\} = \sum_{\nu n} \rho_{\nu n, n-1}^{\nu \nu}(t) \sqrt{n}. \quad (9)$$

Furthermore, as we show in Sec. S.I of the Supplemental Material [26], the pulse operator $\hat{X}(E)$ with a complex pulse area $E = |E|e^{i\varphi}$ transforms the elements $\rho_{nn'}^{\nu \nu'}$ of the DM according to

$$[\hat{X}(E)\rho]_{nn'}^{\nu \nu'} = \sum_{kk'} e^{i\varphi(n-k-n'+k')} C_{nk} C_{n'k'}^* \rho_{kk'}^{\nu \nu'} \quad (10)$$

with the transformation matrix having the *analytic* form

$$C_{nk} = i^{n-k} |E|^{n-k} \sqrt{\frac{k!}{n!}} L_k^{n-k}(|E|^2) e^{-|E|^2/2}, \quad (11)$$

where $L_k^p(x)$ are the associated Laguerre polynomials.

The phase factor in Eq. (10) determines the phase Φ of the optical response, which in turn fixes the number of steps $\mathcal{S} = \nu + n - (\nu' + n')$ between the rungs involved in the coherent dynamics. Even starting from the ground state $\rho_0 = |0, 0\rangle \langle 0, 0|$, an optical pulse distributes the excitation across all rungs of the JC ladder. However, choosing a particular phase $\Phi = \varphi\mathcal{S}$, the subsequent Lindblad evolution does not mix elements of the DM corresponding to different \mathcal{S} .

Similarly, with a number J of pulses exciting the system, all phase channels can be treated independently, so that one can select a phase $\Phi = \sum_{j=1}^J \mathcal{S}_j \varphi_j$ of the optical polarization, determining the transitions between rungs present in

the coherent dynamics following the pulses. These rungs of the JC ladder are separated by a distance $\sum_{j=1}^J \mathcal{S}_j$. In the standard FWM polarization, excited by a sequence of three pulses, the selected phase channel after all pulses is given by $\Phi = \varphi_2 + \varphi_3 - \varphi_1$, corresponding to $\mathcal{S}_1 = -1$ and $\mathcal{S}_2 = \mathcal{S}_3 = 1$, and thus involving transitions between neighboring rungs only. The evolution of the system between pulses ($t < 0$) and after pulses ($t > 0$) keeps phase selection and can also be described by explicit analytic expressions. Introducing a vector $\vec{\rho}$ comprising all relevant elements of the DM, i.e., those involved in the coherent dynamics for the selected phase, the time evolution after pulses is given by

$$\vec{\rho}(t) = e^{-i\hat{L}t}\vec{\rho}(0_+) = \hat{U}e^{-i\hat{\Omega}t}\hat{V}\vec{\rho}(0_+), \quad (12)$$

where the matrices \hat{U} and \hat{V} diagonalizing the Lindblad matrix $\hat{L} = \hat{U}\hat{\Omega}\hat{V}$ take an *analytic* form (see the Supplemental Material [26], Sec. S.III) in terms of 2×2 matrices Y_N diagonalizing the complex Hamiltonian H_N of the N th rung,

$$\begin{aligned} H_N &= \begin{bmatrix} \omega_X + (N-1)\omega_C & \sqrt{N}g \\ \sqrt{N}g & N\omega_C \end{bmatrix} \\ &= Y_N \begin{bmatrix} \lambda_N^- & 0 \\ 0 & \lambda_N^+ \end{bmatrix} Y_N^T, \end{aligned} \quad (13)$$

where λ_N^\pm are the complex eigenvalues of H_N . The diagonal matrix $\hat{\Omega}$ in Eq. (12) consists of the eigenvalues of \hat{L} which are given by $\omega_r = \lambda_{N+S}^s - (\lambda_N^{s'})^*$, with a fixed \mathcal{S} and all possible sign combinations of $s, s' = \pm$ and rung numbers N , including the case of the ground state with $\lambda_0 = 0$. Consequently, the optical polarization in Eq. (9) and its Fourier transform take the analytic form

$$P(t > 0) = \sum_r A_r e^{-i\omega_r t}, \quad \tilde{P}(\omega) = \sum_r \frac{iA_r}{\omega - \omega_r} \quad (14)$$

with the amplitudes $A_r = \sum_{i,j} (\vec{a})_i (\hat{U})_{ir} (\hat{V})_{rj} (\vec{\rho})_j$, according to Eqs. (9) and (12).

We consider below a general case of \mathcal{N} -wave mixing (\mathcal{N} WM) cavity polarization and nonlinear spectrum given by Eq. (14). While the formalism described above is developed for any number of excitation pulses and arbitrary delay times between them, we focus here on degenerate \mathcal{N} WM, generated by two optical pulses with complex pulse areas E_1 and E_2 , so that $\mathcal{N} = |\mathcal{S}_1| + |\mathcal{S}_2| + 1$ with $\mathcal{S} = \mathcal{S}_1 + \mathcal{S}_2 = 1$. The optical response of the system carries a phase $\Phi = \mathcal{S}_1\varphi_1 + \mathcal{S}_2\varphi_2$ (FWM corresponds to $\Phi = 2\varphi_2 - \varphi_1$, with $\mathcal{N} = 4$) and in the low-excitation regime is proportional to a factor $ie^{i\Phi}|E_1|^{|\mathcal{S}_1|}|E_2|^{|\mathcal{S}_2|}$ which we drop in all the results presented below. We assume for simplicity zero delay between the pulses and focus on the

case of $|E_2| \ll 1$, arbitrary E_1 , and zero detuning $\Omega_X = \Omega_C$. The cases $|E_1| \ll 1$ and arbitrary E_2 , and $|E_1| = |E_2|$, as well as nonzero detuning, are considered in the Supplemental Material [26], Sec. S.IX. In the below analytics we use $\Omega_C = 0$ for brevity.

The FWM spectrum $\tilde{P}(\omega)$ calculated for $\gamma_C = g/2$ is shown in Fig. 1(a) as a phase-amplitude color map for the pulse area $0 \leq |E_1| \leq 10$, exciting an average of up to 100 photons. $|\tilde{P}(\omega)|$ is displayed in Fig. 1(c) for selected $|E_1|$, and the optical transitions between neighboring rungs which contribute to these spectra are shown in Figs. 1(d)–1(f) in terms of the complex transition amplitudes A_r and their frequencies ω_r . In the low-excitation regime ($|E_1| = 10^{-3}$), only the first two rungs contribute, and the spectrum in Fig. 1(c) shows a doublet due to the lowest-rung transitions, studied in detail in Ref. [10]. For $|E_1| = 2$, the spectrum is wider, having a central peak and

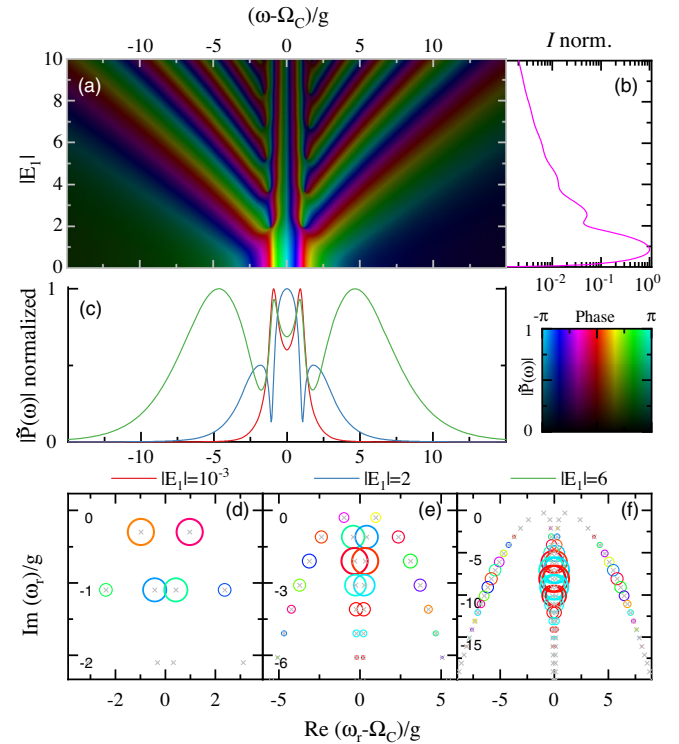


FIG. 1. FWM response calculated for $|E_2| = 0.001$ and varying $|E_1|$, with $\Omega_X = \Omega_C$, $\gamma_C = g/2$, and $\gamma_X = g/10$ corresponding to the experiments reported in Refs. [10,23–25]. (a) FWM spectrum $\tilde{P}(\omega)$ in a color plot with the hue giving the phase (see color scale) and the brightness giving the amplitude $|\tilde{P}|^{1/4}$. (b) Spectrally integrated power $I = \int |\tilde{P}(\omega)|^2 d\omega$ versus $|E_1|$ (For more on power see the Supplemental Material [26], Sec. S.VIII). (c) $|\tilde{P}(\omega)|$ normalized to 1, for selected $|E_1|$ as labeled. (d)–(f) Optical transition frequencies ω_r and their complex amplitudes A_r in $\tilde{P}(\omega)$ [see Eq. (14)], for different $|E_1|$ as given in (c). ω_r and A_r are shown, respectively, by crosses in the complex ω plane and by circles centered at ω_r with area proportional to $|A_r|$ and color given by the phase of A_r , according to the scale in (a).

sidebands, formed by a range of transitions strongest for rungs 1–5. For $|E_1| = 6$, an outer doublet of increased separation and strength develops, the inner doublet reappears, and a large number of rungs are involved.

The transition frequencies are given by $\omega_r = \pm\Delta_n^\sigma - i(2n\gamma_C + \gamma_X)$, where $\sigma = o, i$, and n is the rung number. For each rung $n > 1$, there are two “inner” and two “outer” transitions, corresponding to $\Delta_n^i = (\sqrt{n+1} - \sqrt{n})g$ and $\Delta_n^o = (\sqrt{n+1} + \sqrt{n})g$, respectively (for $\gamma_X = \gamma_C$). Neglecting relaxation, the system excited with $|E_1|^2$ photons has a dominant contribution coming from rungs with $n \sim |E_1|^2$. This implies that as E_1 increases, the spectrum can consist of an inner doublet due to the inner transitions at $\omega \approx \pm\Delta_n^i$, close to zero, and an outer doublet at $\omega \approx \pm\Delta_n^o \approx \pm 2g|E_1|$, thus forming the QMQ. Such a spectrum differs from the MT observed in a two-level system continuously driven by a classical light [13], by the formation of the inner doublet and the intrinsic linewidths, as we will see later. The separation of the outer doublet of $\tilde{P}(\omega)$ in Fig. 1(a) grows almost linearly with $|E_1|$, similar to the sidebands in the MT. However, the observed splitting is somewhat smaller than $4g|E_1|$. A closer look into the complex transition amplitudes (see the Supplemental Material [26], Sec. S.VI.) reveals a Poisson-like distribution peaked at a rung number lower than excited ($n = |E_1|^2 = 36$), which is caused by relaxation, and a significant destructive interference between the transitions.

To better understand the observed QMQ, we develop an analytic approach to the \mathcal{N} WM response with $S_1 = 1 - \mathcal{N}/2$ and $S_2 = \mathcal{N}/2 \equiv m$ in the limit of low damping ($\gamma_X, \gamma_C \ll g$), as detailed in the Supplemental Material [26], Sec. S.V. In the limit of large pulse area, $\lambda \equiv |E_1|^2 \gg 1$, the Poisson distribution with λ in Eq. (10) becomes approximately Gaussian, with the mean rung number given by the mean photon number, $\langle n \rangle = \lambda$, and the mean square deviation $\langle n^2 - \lambda^2 \rangle = \lambda$. Around the maximum of this distribution, the Laguerre polynomials are approximated by Hermite polynomials, and the frequencies of the inner and outer transitions by

$$\Delta_n^o \approx 2\sqrt{\lambda}g + z\sqrt{2}g, \quad \Delta_n^i \approx \frac{g}{2\sqrt{\lambda}} - z\frac{g}{2\sqrt{2}\lambda}, \quad (15)$$

where $z = (n - \lambda)/\sqrt{2\lambda}$ (see the Supplemental Material [26], Secs. S.IV and S.V.) This allows us to replace the transition frequencies in Eq. (14) with $\omega_r = s\Delta_n^\sigma \approx \omega_{\sigma s} + z\gamma_{\sigma s}$, where the frequencies $\omega_{\sigma s}$ and the linewidths $\gamma_{\sigma s}$ are defined by Eq. (15), and $s = \pm$. Note that the linewidth $\gamma_{\sigma s}$ is produced by a coherent superposition of many inner or outer transitions and is thus determined by their frequency dispersion with respect to the rung number n . The coherent dynamics after pulses can then be treated analytically, replacing $\sum_n \rightarrow \sqrt{2\lambda} \int dz$ in Eq. (9), which results in the explicit form of the \mathcal{N} WM polarization:

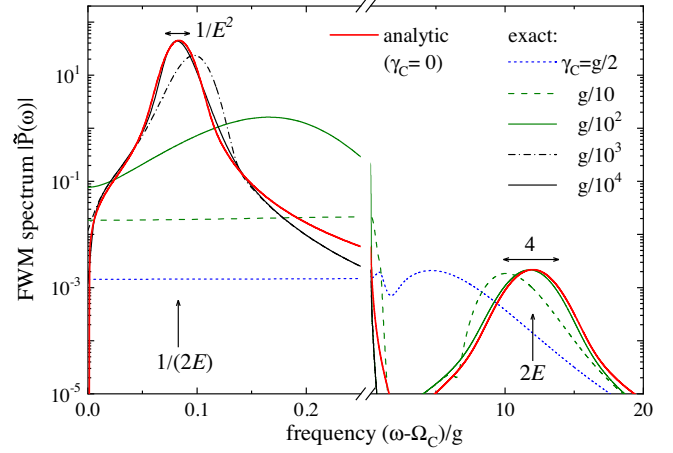


FIG. 2. Analytic approximation Eq. (17) (red curve) and exact FWM spectrum for different γ_C as given, for $E = \sqrt{\lambda} = |E_1| = 6$. Vertical (horizontal) arrows show the position and FWHM of the spectral lines produced by the inner and outer transitions.

$$P(t) = \sum_{\sigma=i,o} \sum_{s=\pm} \frac{1}{2} A_\sigma^{(m)} (\gamma_{\sigma s} t)^m e^{-i\omega_{\sigma s} t - (\gamma_{\sigma s} t)^2/4}, \quad (16)$$

where $A_o^{(m)} = (-i)^m / [4m! (\sqrt{2\lambda})^m]$ and $A_i^{(m)} = 4\lambda A_o^{(m)}$. Fourier transforming Eq. (16) gives an *analytic* \mathcal{N} WM spectrum

$$\begin{aligned} \tilde{P}(\omega) &= \frac{(-i)^m}{4m! (\sqrt{2\lambda})^m} [\tilde{P}(\omega) + \tilde{P}^*(-\omega)], \\ \tilde{P}(\omega) &= w_m \left(\frac{\omega - \sqrt{4\lambda}g}{\sqrt{2}g} \right) + 16\lambda^2 w_m \left(4\lambda \frac{\omega + g/\sqrt{4\lambda}}{\sqrt{2}g} \right), \end{aligned} \quad (17)$$

where $w_m(z) = \frac{1}{2} \int_0^\infty t^m e^{izt} e^{-t^2/4} dt$ is a generalized Faddeeva function. Equation (17) also holds for the case of small E_1

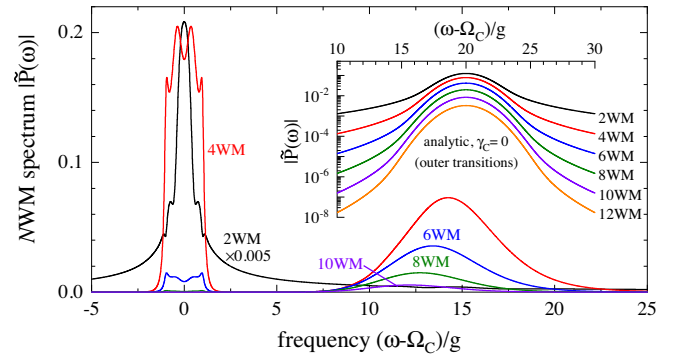


FIG. 3. \mathcal{N} WM spectra $|\tilde{P}(\omega)|$ of the response detected at $\Phi = \varphi_1$ ($\mathcal{N} = 2$, black), $2\varphi_2 - \varphi_1$ ($\mathcal{N} = 4$, red), $3\varphi_2 - 2\varphi_1$ ($\mathcal{N} = 6$, blue), and $4\varphi_2 - 3\varphi_1$ ($\mathcal{N} = 8$, green), for $|E_1| = 10$ and $\gamma_C = g/5$. Inset: spectral line of the outer doublet of the QMQ for \mathcal{N} up to 12, calculated using the analytic approximation Eq. (17). All spectra are multiplied by $|E_1|^{\mathcal{N}/2}$.

and large E_2 , by using instead $\lambda = |E_2|^2$, $m = \mathcal{N}/2 - 1$, and dividing $\bar{P}(\omega)$ by λ .

Figure 2 illustrates the analytic approximation Eq. (17) for $|E_1| = 6$, in comparison with the full calculation at different values of γ_C , demonstrating good agreement for small damping. Note that the value of $\gamma_C = g/10$ has been recently observed in a QD-cavity system [32]. The first term in \bar{P} , produced by the outer transitions, describes the outer doublet of the QMQ, with a maximum at $\omega = \sqrt{4\lambda}g = 2g|E_1|$ and a linewidth of $\sqrt{2}g$, corresponding to a full width at half maximum (FWHM) of about $4g$. The linewidth is independent of the pulse area, which is also seen in the full calculation even for a rather large damping. This can be understood from the dispersion of the outer transitions, with the peak frequency at $\sim 2g\sqrt{\lambda}$ and the Gaussian distribution of transition amplitudes with the root-mean-square width of $\sqrt{\lambda}$, leading to spectral width of $\sim g$, independent of λ . The inner transitions are in turn responsible for the inner doublet of the QMQ, which is replacing the central line of the MT. Its peak position $g/\sqrt{4\lambda}$ and FWHM g/λ both decrease with pulse area. Notably, the relative amplitude of inner to outer doublet scales as λ^2 , so that the inner doublet dominates at high pulse areas.

Let us now consider higher-order \mathcal{N} WM presented in Fig. 3. The inset shows the analytic spectrum of the outer transitions for $\mathcal{N} = 2, 4, 6, 8, 10$, and 12. While the FWHM almost does not change with \mathcal{N} , the spectral tails are increasingly suppressed, which can be seen in the time domain as a $t^{\mathcal{N}/2}$ rise of the polarization at short times [see Eq. (16)]. The increase with \mathcal{N} of the rise time is due to the fact that the optical nonlinearity requires the excitation to be transferred from the CM to the TLS and then back to the cavity, with the number of such loops increasing with \mathcal{N} . The outer doublet is prominent in the FWM spectrum, and dominates over the central band starting from 6WM (for the chosen parameters).

In conclusion, we find that a dramatic interference of the spectrally dense transitions of a Jaynes-Cummings ladder results in a remarkable effect in nonlinear optical spectra: the formation of a quantum Mollow quadruplet.

The supporting data for this article are openly available from [37].

T. A. acknowledges support by a PhD studentship funded by Cardiff University. This work was supported by the EPSRC under Grant No. EP/M020479/1.

-
- [1] J. J. Hopfield, Theory of the contribution of excitons to the complex dielectric constant of crystals, *Phys. Rev.* **112**, 1555 (1958).
 [2] C. Weisbuch, M. Nishioka, A. Ishikawa, and Y. Arakawa, Observation of the Coupled Exciton-Photon Mode Splitting

- in a Semiconductor Quantum Microcavity, *Phys. Rev. Lett.* **69**, 3314 (1992).
 [3] C. J. Hood, M. S. Chapman, T. W. Lynn, and H. J. Kimble, Real-Time Cavity QED with Single Atoms, *Phys. Rev. Lett.* **80**, 4157 (1998).
 [4] J. P. Reithmaier, G. Sęk, A. Löffler, C. Hoffmann, S. Kuhn, S. Reitzenstein, L. V. Keldysh, V. D. Kulakovskii, T. L. Reinecke, and A. Forchel, Strong coupling in a single quantum dot-semiconductor microcavity system, *Nature (London)* **432**, 197 (2004).
 [5] T. Yoshie, A. Scherer, J. Hendrickson, G. Khitrova, H. M. Gibbs, G. Rupper, C. Ell, O. B. Shchekin, and D. G. Deppe, Vacuum Rabi splitting with a single quantum dot in a photonic crystal nanocavity, *Nature (London)* **432**, 200 (2004).
 [6] J. M. Fink, M. Goppl, M. Baur, R. Bianchetti, P. J. Leek, A. Blais, and A. Wallraff, Climbing the Jaynes-Cummings ladder and observing its nonlinearity in a cavity QED system, *Nature (London)* **454**, 315 (2008).
 [7] L. S. Bishop, J. M. Chow, J. Koch, A. A. Houck, M. H. Devoret, E. Thuneberg, S. M. Girvin, and R. J. Schoelkopf, Nonlinear response of the vacuum Rabi resonance, *Nat. Phys.* **5**, 105 (2009).
 [8] K. M. Birnbaum, A. Boca, R. Miller, A. D. Boozer, T. E. Northup, and H. J. Kimble, Photon blockade in an optical cavity with one trapped atom, *Nature (London)* **436**, 87 (2005).
 [9] I. Schuster, A. Kubanek, A. Fuhrmanek, T. Puppe, P. W. H. Pinkse, K. Murr, and G. Rempe, Nonlinear spectroscopy of photons bound to one atom, *Nat. Phys.* **4**, 382 (2008).
 [10] J. Kasprzak, S. Reitzenstein, E. A. Muljarov, C. Kistner, C. Schneider, M. Strauss, S. Höfling, A. Forchel, and W. Langbein, Up on the Jaynes-Cummings ladder of a quantum-dot/microcavity system, *Nat. Mater.* **9**, 304 (2010).
 [11] E. Jaynes and F. Cummings, Comparison of quantum and semiclassical radiation theories with application to the beam maser., *Proc. IEEE* **51**, 89 (1963).
 [12] A. Faraon, I. Fushman, D. Englund, N. Stoltz, P. Petroff, and J. Vuckovic, Coherent generation of non-classical light on a chip via photon-induced tunnelling and blockade, *Nat. Phys.* **4**, 859 (2008).
 [13] B. R. Mollow, Power spectrum of light scattered by two-level systems, *Phys. Rev.* **188**, 1969 (1969).
 [14] A. Müller, E. B. Flagg, P. Bianucci, X. Y. Wang, D. G. Deppe, W. Ma, J. Zhang, G. J. Salamo, M. Xiao, and C. K. Shih, Resonance Fluorescence from a Coherently Driven Semiconductor Quantum Dot in a Cavity, *Phys. Rev. Lett.* **99**, 187402 (2007).
 [15] S. Ates, S. M. Ulrich, S. Reitzenstein, A. Löffler, A. Forchel, and P. Michler, Post-Selected Indistinguishable Photons from the Resonance Fluorescence of a Single Quantum Dot in a Microcavity, *Phys. Rev. Lett.* **103**, 167402 (2009).
 [16] A. N. Vamivakas, Y. Zhao, C.-Y. Lu, and M. Atatüre, Spin-resolved quantum-dot resonance fluorescence, *Nat. Phys.* **5**, 925 (2009).
 [17] E. B. Flagg, A. Müller, J. W. Robertson, S. Founta, D. G. Deppe, M. Xiao, W. Ma, G. J. Salamo, and C. K. Shih, Resonantly driven coherent oscillations in a solid-state quantum emitter, *Nat. Phys.* **5**, 203 (2009).

- [18] O. Astafiev, A. M. Zagoskin, A. A. Abdumalikov, Y. A. Pashkin, T. Yamamoto, K. Inomata, Y. Nakamura, and J. S. Tsai, Resonance fluorescence of a single artificial atom, *Science* **327**, 840 (2010).
- [19] F. P. Laussy, M. M. Glazov, A. Kavokin, D. M. Whittaker, and G. Malpuech, Statistics of excitons in quantum dots and their effect on the optical emission spectra of microcavities, *Phys. Rev. B* **73**, 115343 (2006).
- [20] E. del Valle, F. P. Laussy, and C. Tejedor, Luminescence spectra of quantum dots in microcavities. II. Fermions, *Phys. Rev. B* **79**, 235326 (2009).
- [21] E. del Valle and F. P. Laussy, Mollow Triplet Under Incoherent Pumping, *Phys. Rev. Lett.* **105**, 233601 (2010).
- [22] W. Langbein and B. Patton, Heterodyne spectral interferometry for multidimensional nonlinear spectroscopy of individual quantum systems, *Opt. Lett.* **31**, 1151 (2006).
- [23] J. Kasprzak, K. Sivalertporn, F. Albert, C. Schneider, S. Höfling, M. Kamp, A. Forchel, S. Reitzenstein, E. A. Muljarov, and W. Langbein, Coherence dynamics and quantum-to-classical crossover in an exciton-cavity system in the quantum strong coupling regime, *New J. Phys.* **15**, 045013 (2013).
- [24] F. Albert, K. Sivalertporn, J. Kasprzak, M. Strauß, C. Schneider, S. Höfling, M. Kamp, A. Forchel, S. Reitzenstein, E. A. Muljarov, and W. Langbein, Microcavity controlled coupling of excitonic qubits, *Nat. Commun.* **4**, 1747 (2013).
- [25] D. Groll, D. Wigger, K. Jürgens, T. Hahn, C. Schneider, M. Kamp, S. Höfling, J. Kasprzak, and T. Kuhn, Four-wave mixing dynamics of a strongly coupled quantum-dot–microcavity system driven by up to 20 photons, *Phys. Rev. B* **101**, 245301 (2020).
- [26] See Supplemental Material at <http://link.aps.org/supplemental/10.1103/PhysRevLett.128.123602> for a full derivation of the analytical results of this Letter, justification of our choice of JC model parameters, details on numerical convergence and use of multiple precision arithmetic, and a collection of more results on the FWM spectra similar to Fig. 1, which includes [27–34].
- [27] M. Suzuki, Generalized Trotter’s formula and systematic approximants of exponential operators and inner derivations with applications to many-body problems, *Commun. Math. Phys.* **51**, 183 (1976).
- [28] I. S. Gradshteyn and I. M. Ryzhik, *Table of Integrals, Series, and Products* (Academic Press, New York, 1965).
- [29] E. Peter, P. Senellart, D. Martrou, A. Lemaître, J. Hours, J. M. Gérard, and J. Bloch, Exciton-Photon Strong-Coupling Regime for a Single Quantum Dot Embedded in a Microcavity, *Phys. Rev. Lett.* **95**, 067401 (2005).
- [30] R. Ohta, Y. Ota, M. Nomura, N. Kumagai, S. Ishida, S. Iwamoto, and Y. Arakawa, Strong coupling between a photonic crystal nanobeam cavity and a single quantum dot, *Appl. Phys. Lett.* **98**, 173104 (2011).
- [31] B. Guha, F. Marsault, F. Cadiz, L. Morgenroth, V. Ulin, V. Berkovitz, A. Lemaître, C. Gomez, A. Amo, S. Combrié, B. Gérard, G. Leo, and I. Favero, Surface-enhanced gallium arsenide photonic resonator with quality factor of 6×10^6 , *Optica* **4**, 218 (2017).
- [32] D. Najer, I. Sllner, P. Sekatski, V. Dolique, M. C. Lbl, D. Riedel, R. Schott, S. Starosielec, S. R. Valentin, A. D. Wieck, N. Sangouard, A. Ludwig, and R. J. Warburton, A gated quantum dot strongly coupled to an optical microcavity, *Nature (London)* **575**, 622 (2019).
- [33] A. Morreau and E. A. Muljarov, Phonon-induced dephasing in quantum-dot–cavity QED, *Phys. Rev. B* **100**, 115309 (2019).
- [34] E. A. Muljarov and R. Zimmermann, Dephasing in Quantum Dots: Quadratic Coupling to Acoustic Phonons, *Phys. Rev. Lett.* **93**, 237401 (2004).
- [35] H. M. Wiseman and G. J. Milburn, *Quantum Measurement and Control* (Cambridge University Press, Cambridge, England, 2009).
- [36] R. J. Glauber, Coherent and incoherent states of the radiation field, *Phys. Rev.* **131**, 2766 (1963).
- [37] [10.17035/d.2022.0161505679](https://doi.org/10.17035/d.2022.0161505679).